RSC Advances

PAPER

50–100 μm-thick pseudocapacitive electrodes of MnO₂ nanoparticles uniformly electrodeposited in carbon nanotube papers†

Misato Narubayashi, Zhongming Chen, Kei Hasegawa and Suguru Noda*

To overcome the tradeoff between the gravimetric capacitance and loading density of pseudocapacitive MnO_2, we electrodeposited MnO_2 nanoparticles on the carbon nanotube (CNT) surfaces in 18–37 μm-thick self-supporting CNT papers. We examined the electrodeposition conditions including constant potential, constant current, and potential pulses, and obtained MnO_2–CNT hybrid electrodes containing MnO_2 nanoparticles uniformly deposited at 60–90 wt% with an expanded CNT matrix. The MnO_2–CNT hybrid electrode with a thickness of 62 μm, density of 1.09 g cm^{-3}, areal mass of 6.75 mg cm^{-2}, and 82 wt% MnO_2 load showed a total gravimetric capacitance of 120 and 51 F_{total} $g_{electrode}^{-1}$, volumetric capacitance of 131 and 56 F_{total} cm^{-3} and areal capacitance of 0.81 and 0.34 F_{total} cm^{-2} at scan rates of 2 and 200 mV s^{-1}, respectively. The large thickness, moderately high mass density, and fairly conductive CNT matrix realized such high values of gravimetric, areal and volumetric capacitances that are important for practical devices.

Introduction

In recent years, owing to the growing demand for normalizing power fluctuations of solar and wind power generation and energy recovery in automobiles, electrochemical capacitors have attracted increasing attention as high power electrochemical energy storage devices. Activated carbon (AC), which has a huge specific surface area, is generally used as an active material for electric double layer capacitors, but there is limited room to enhance the capacitance by controlling the pore size distribution. To enhance the energy densities, pseudocapacitors using redox reactions of active materials such as metal oxides and conductive polymers, have been extensively studied. Ru compounds have been studied most extensively as active materials because they have high conductivity, proton mobility, and high capacitance in a wide potential window.[1–3] It was reported that amorphous ruthenium oxide material calcined at 150 °C showed a maximum capacitance of 720 F g^{-1} in sulfuric acid electrolyte,[1] and crystalline ruthenium oxide calcined at 200 °C showed a maximum capacitance of 710 F g^{-1} in KOH electrolyte.[4] However, because ruthenium is a rare metal with a high cost and toxicity, less expensive materials have been studied.[5] MnO_2, with a high theoretical capacity of 1100 C g^{-1}, is a promising candidate as an active material for commercial use because it is abundant, inexpensive, and environmentally

friendly.[6] However, it is necessary to use fine MnO_2 particles with a high specific surface area because the conductivity of MnO_2 is low and the redox reaction occurs preferentially on or near the surface during charge and discharge (eqn (1)).[7]

$$MnOOA \rightleftarrows MnO_2 + A^+ + e^- \tag{1}$$

A very high gravimetric capacitance of 1200 F $g_{MnO_2}^{-1}$ at 3 mV s^{-1} was confirmed,[8] but for a very thin layer on indium tin oxide-coated glass substrate, resulting in a very small areal capacitance of 6.8×10^{-4} F cm^{-2}.

Conventional capacitor electrodes are built on current collectors of metal foils on which active materials are attached by binders with conductive fillers (Fig. 1a). Although high gravimetric capacitance values have been reported for thin MnO_2 electrodes (Fig. 1b), the capacitance per device is small because of the much larger mass of the current collector and separator compared with the active materials. In contrast, the gravimetric capacitance values of thick MnO_2 electrodes are small (Fig. 1c). To utilize fine MnO_2 particles at higher loads, their composites with carbon materials including carbon nanotubes (CNTs) or conductive polymers have also been studied.[9–14]

CNTs are a conductive material with high aspect ratios and specific surface areas, high tensile strength with flexibility, and high thermal and chemical stability, and are expected to be applied in various electric and electronic devices. We have developed a fluidized bed chemical vapour deposition method that enables semi-continuous production of 200–400 μm-long few-wall CNTs with an average diameter of 6.5–8 nm, carbon

Department of Applied Chemistry, Waseda University, 3-4-1 Okubo, Shinjuku-ku, Tokyo 169-8555, Japan. E-mail: noda@waseda.jp
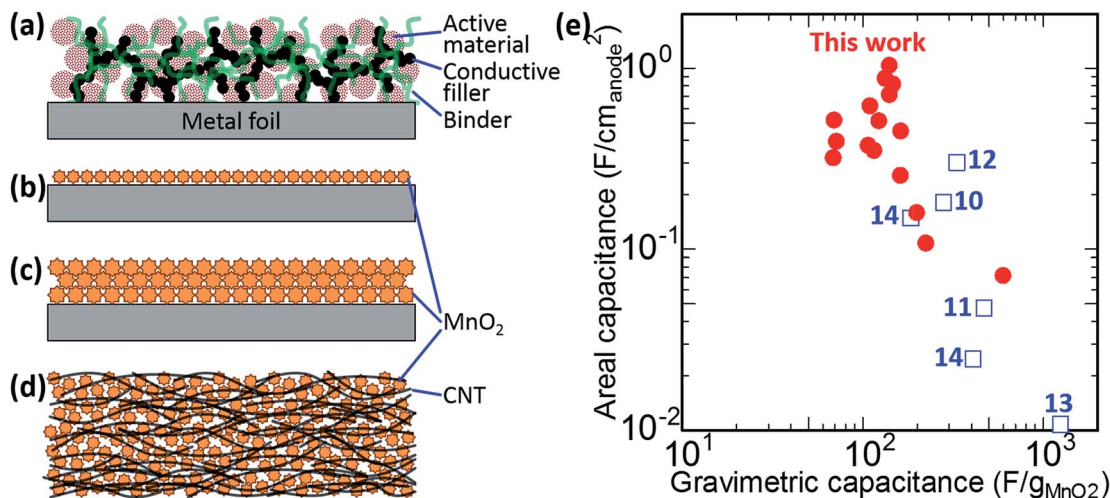
Fig. 1 Schematic illustrations of (a) conventional electric double layer capacitor electrode, (b) thin MnO_2 electrode, (c) thick MnO_2 electrode, and (d) the proposed MnO_2–CNT hybrid electrode. (e) Gravimetric and areal capacitances of MnO_2-based electrodes of previous works (blue open squares; the numbers represent the references)[10–14] with scan rates of 1.25–20 mV s^{-1} and the present work (red closed circles) with a scan rate of 2 mV s^{-1}. The capacitance values shown are for the total capacitance of the electrodes.

purity of over 99 wt%, and a specific surface area of 400–440 m^2 g^{-1}.[15,16] Such CNTs can form self-supporting papers with arbitrary thicknesses through a simple dispersion–filtration process without any binding additives. The CNT papers have a much larger surface area (2000–6000 cm^2 for 20–60 μm-thick, 1 cm^2 CNT paper) than metal foils (2 cm^2 surface area for 1 cm^2 foil) and can capture various active materials inside their nanometre-sized pores at loads much larger than their own mass. Positive electrodes of oxidized CNT papers for lithium batteries,[17] positive electrodes of polymerized pyrene derivatives held in CNT papers for pseudocapacitors,[18] and biomass-derived carbonaceous positive electrodes for lithium cells[19] have been realized. We have also realized a self-supporting paper of AC (90 wt%) held by CNTs (10 wt%), which showed a three-times higher specific capacitance than the pure single-wall CNT electrodes[20] and worked as a capacitor electrode not only in full contact but also in line contact to a metal mesh.[21]

The practical use of MnO_2 as an active material in electrochemical capacitors requires: (1) deposition of fine MnO_2 particles at a high density, (2) building of conductive paths to all MnO_2 particles, and (3) electrodes that are sufficiently thick (several tens of micrometres). In this study, we aimed to fabricate electrodes using MnO_2–CNT hybrids that have a high capacitance per mass and area of the electrode (Fig. 1d). Various methods such as hydrothermal synthesis,[22] sol–gel method,[23] electrostatic spray deposition,[24] electrophoretic deposition,[25] anodic oxidation,[26] and cathodic reduction[27] have been reported for making MnO_2. Among them, electrodeposition[26,27] is attractive because it forms conductive paths to every MnO_2 particle. Uniform deposition of nickel oxide particles in vertically aligned CNT forests have been reported although the volumetric capacitance was small (1.26 F cm^{-3}).[28] Therefore, we electrodeposited MnO_2 directly on CNT papers by anodically oxidizing Mn^{2+} ions using the CNT papers as a working electrode in a $MnSO_4$ aqueous solution. A high potential is needed

to deposit small MnO_2 particles at a high density by enhancing their nucleation. But at the same time, high potential leads to a high deposition rate and diffusion-limited deposition, resulting in the preferential deposition of MnO_2 on the outer surface of thick CNT papers. We examined electrodeposition at a constant potential (CP), at a constant current (CC), or by applying high potential pulses (hereafter "Pulse"), and analysed micro- and macroscopic structural changes and charge–discharge characteristics. The thick MnO_2–CNT hybrids reported here have a higher areal capacitance than any previous report on MnO_2 (Fig. 1e), expect for the very high value of 2.8 F cm^{-2} recorded at a very small scan rate of 0.05 mV s^{-1} for MnO_2–CNT-textile with a high MnO_2 load of 8.3 mg cm^{-2}.[14]

Experimental

Preparation of the MnO_2–CNT hybrid papers

Sub-millimetre-long few-wall CNTs (3–10 mg) synthesized by fluidized bed chemical vapour deposition[16] were mixed with a 0.5 wt% sodium dodecylbenzene sulfonate aqueous solution (30–100 mL) and dispersed by ultrasonication (bath-type, 100 W, 30–100 min). The dispersed CNT solution was vacuum-filtrated on a membrane filter (polytetrafluoroethylene, pore size of 0.5 μm), and the CNT film on the membrane filter was washed by hot distilled water (80 °C), dried at 90 °C for 2 h under air, and then separated from the membrane filter using tweezers. The areal mass of the CNTs was controlled at 0.6–1.4 mg cm^{-2}, yielding self-supporting CNT papers with a mass density of 0.25–0.48 g cm^{-3} and a thickness of 18–37 μm. MnO_2–CNT hybrids were then prepared by electrodeposition using the condition reported by Jin et al.[29] MnO_2 were deposited on/in the CNT paper immersed in 0.6 M $MnSO_4$/0.8 M H_2SO_4 aqueous electrolyte using the CNT paper as a working electrode, a graphite sheet as a counter electrode, and Ag/AgCl electrode (in 3 M NaCl aqueous solution) as a reference electrode. The

electrodeposition was conducted either at CP, CC, or Pulse. The obtained electrodes were dried at 90 °C for 2 h under air.

Characterization of the MnO$_2$–CNT hybrids

The microstructure of the MnO$_2$–CNT hybrids was characterized using a scanning electron microscope (SEM, Hitachi S-4800, Tokyo, Japan). The composition of the MnO$_2$–CNT hybrids was evaluated using energy-dispersive X-ray spectroscopy (EDAX Genesis, AMETEK, Elancourt, France) equipped to SEM and mass change of the CNT papers. Their crystal structure was analysed using X-ray diffraction (Ultima III system, Rigaku, Akishima, Japan). Three-electrode cells were used to run cyclic voltammetry (CV), electrochemical impedance spectroscopy, and galvanostatic charge–discharge tests with a VMP3 potentiostat (Bio-Logic, Grenoble, France). The three-electrode cell consisted of a hybrid electrode as the working electrode, an AC–CNT hybrid film (90 wt% AC with 10 wt% CNTs, ~200 μm in thickness)[21] as the counter electrode and an Ag/AgCl electrode (in 3 M NaCl aqueous solution) as the reference electrode with 1 M Na$_2$SO$_4$ aqueous solution as the electrolyte. Structure and electrochemical performance are summarized for all and representative samples in ESI Tables S1 and S2, respectively.†

Results and discussion

Rate process of electrodeposition and microstructure of the resulting MnO$_2$ in CNT papers

Fig. S1† shows the typical current behaviour during electrodeposition of MnO$_2$ at a potential range of 0.0–2.0 V. All potential values are shown vs. Ag/AgCl throughout this report. The equilibrium electrode potential of the CNT paper in the 0.6 M MnSO$_4$/0.8 M H$_2$SO$_4$ aqueous electrolyte is 1.05 V. A rise in the current was observed twice at approximately 1.15 and 1.7 V, which possibly corresponds to the oxidation of Mn^{2+} ions (deposition of MnO$_2$ onto the CNT paper) and further oxidation of MnO$_2$ to MnO$_4^-$ ions (resulting in the dissolution of deposited MnO$_2$), respectively. The deposition rate of MnO$_2$ is controlled by the potential of the CNT paper. We will discuss each aspect separately in detail below.

Fig. 2a and b shows the current density profiles during electrodeposition at CP of 1.15, 1.20, and 1.30 V against the time of electrodeposition and the integrated electric charge, respectively. At all three potentials, a large current density was initially observed just after applying the electric potential, which quickly decayed in the first several seconds (Fig. 2a). The current density at 1.15 V became very small. Conversely, the current density increased for ~5 and ~2 min, became saturated, and decreased after ~16 and ~5 min at 1.20 and 1.30 V, respectively. Fig. 2c–i shows the plan-view SEM images of the surfaces of the CNT papers before (Fig. 2c) and after (Fig. 2d–i) electrodeposition. Flower-shaped particles formed inside the CNT papers (Fig. 2d, e and g) with increasing size and number density with time (Fig. 2d vs. 2e), and dense layers formed on the surface of the CNT papers after the decrease in the current density (Fig. 2f, h and i). These results suggest that the initial large current density after several seconds corresponds to the charge accumulation

by the electric double layer on the CNT surface. The subsequent increase in current density corresponds to the increasing surface area of MnO$_2$ by nucleation and growth of MnO$_2$ particles and the final decrease in current density corresponds to the decreasing surface area and increasing electric resistance of the dense MnO$_2$ layer. The increase in current density with the nucleation and growth of MnO$_2$ particles indicates that the MnO$_2$ deposition is preferred on the MnO$_2$ surface rather than on the CNT surface. The interior of the CNT paper was filled with MnO$_2$ particles uniformly from top to the bottom of the paper (Fig. 2j–m and S2a†), indicating that the Mn^{2+} diffuses into the CNT paper until the surface of the CNT paper is covered with a dense MnO$_2$ layer. The MnO$_2$ deposition accompanied the expansion of the CNT paper matrix, from 30 to 61–63 μm in thickness with the areal mass increase from 1.23 to 6.75 mg cm^{-2} and density increase from 0.41 to 1.09 g cm^{-3} during 10 min deposition at 1.20 V (Fig. 2j). As the deposition proceeds, the tortuosity of the CNT paper increases whereas the porosity decreases, thereby inhibiting the diffusion of Mn^{2+} and making the deposition of MnO$_2$ preferential at the exterior of the paper and resulting in a dense MnO$_2$ layer. Fig. 2b shows the change of current density with the integrated electric charge (corresponding to the amount of deposited MnO$_2$). The current density decreased at a smaller integrated electric charge of ~10 C cm^{-2} at 1.30 V than at ~17 C cm^{-2} at 1.20 V, showing that less MnO$_2$ nanoparticles can be deposited inside the CNT paper at higher potential owing to the accelerated formation of a dense layer. Comparison of Fig. 2e and g shows that smaller MnO$_2$ particles were deposited at a higher number density at potentials of 1.30 V than at 1.20 V, indicating that a higher potential enhances the nucleation more than the growth of MnO$_2$ particles. To realize high areal capacitance of the hybrid electrode, fine particles must be deposited at a high number density. Here arises a difficult tradeoff; a higher potential is needed to enhance the nucleation density of MnO$_2$ particles, which at the same time causes concentration distribution of Mn^{2+} ions within the CNT papers, resulting in a dense MnO$_2$ layer on the exterior of the CNT papers.

To electrodeposit MnO$_2$ particles in CNT papers uniformly at a high density, we investigated the control of the reaction rate by electrodeposition with CC. Fig. 3a and b shows potential profiles during electrodeposition at CC of 2 and 20 mA cm^{-2}, respectively. At 2 mA cm^{-2}, the potential changed slightly between 1.15 and 1.19 V for 180 min; it initially increased and then decreased and remained at a constant value. At 20 mA cm^{-2}, the potential showed a similar change at ~1.2 V for 10 min (less than 1/10 of that for 2 mA cm^{-2}) and then increased abruptly to ~1.5 V at ~12 min. Fig. 3c shows the change in current density with integrated electric charge. It clearly shows that the MnO$_2$ deposition proceeded at a higher potential with an abrupt potential increase with the larger current density of 20 mA cm^{-2}. Fig. 3d–g shows plan-view SEM images of the surface of the MnO$_2$–CNT hybrids after electrodeposition with CC of 2 mA cm^{-2}. Particles grew continuously without forming a layer on the CNT paper surface even after a long electrodeposition time at 2 mA cm^{-2}. Conversely, at 20 mA cm^{-2}, small MnO$_2$ particles formed at a higher density (Fig. 3h) and a dense
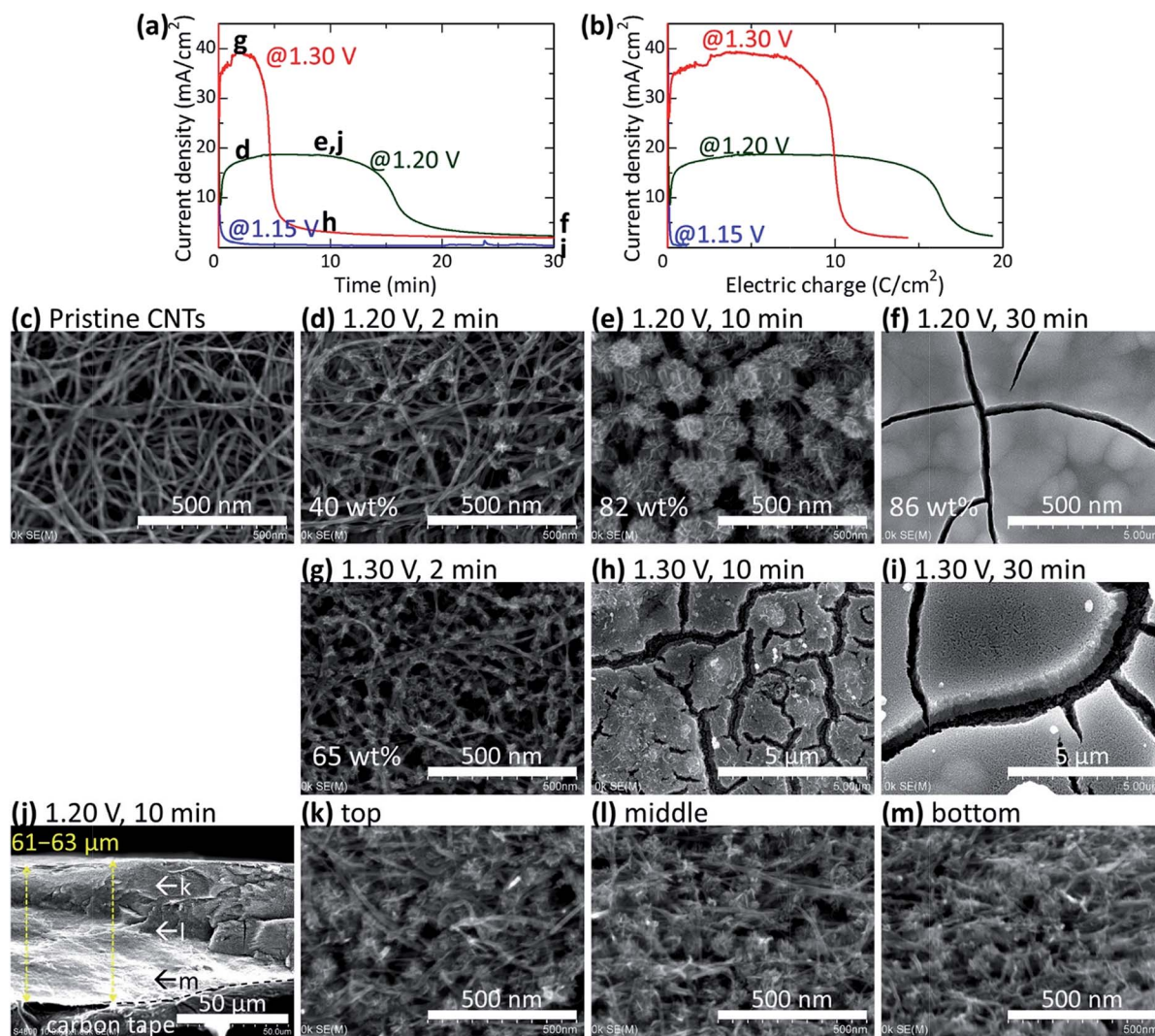
Fig. 2   Electrodeposition of MnO_2 in CNT papers (18–32 μm in thickness) at CP of 1.15, 1.20, and 1.30 V. Current change with (a) electrodeposition time and (b) integrated electric charge. SEM images of the surfaces of the CNT paper before (c) and after (d–i) electrodeposition. Cross-sectional SEM images of (e) is shown in (j–m). SEM-EDS elemental mapping images are shown for the cross-section in Fig. S2a.†

layer formed on the surface of the CNT paper after deposition for 18 min (Fig. 3i). The initial increase, decrease, plateau, and abrupt increase (only with 20 mA cm^{-2}) in the potential correspond to the charge accumulation by double-layer capacitance, the increased reaction area as a result of the formation of the MnO_2 particles, the sufficient surface area for reaction and interspace for diffusion of the growing MnO_2 particles, and the inhibited diffusion owing to the dense layer formation, respectively. It can be said that Mn^{2+} ions can diffuse uniformly even with a large amount of deposited MnO_2 (22 C cm^{-2} and 87 wt%) when MnO_2 is deposited slowly at 2 mA cm^{-2}.

Fig. 3j–m shows the cross-section of the film after electrodeposition at 20 mA cm^{-2} for 9 min (the same film as Fig. 3h). It indicates that MnO_2 particles were uniformly electrodeposited inside the CNT paper. Increased current density (20 mA cm^{-2}) and, thus, the overpotential (~1.2 V) enhances the nucleation of MnO_2 particles, initially making small MnO_2 particles at high density (Fig. 3h and j). However, the potential increases at ~12

min owing to the formation of a surface layer (Fig. 3i); the accessible surface area of MnO_2 for Mn^{2+} ions decreases and the overpotential increases to balance the constant current.

To electrodeposit fine MnO_2 particles at a high density, next we investigated intermittently applying high potential pulses. We expected the nucleation of MnO_2 particles to be accelerated by the high potential, and a uniform deposition of fine MnO_2 particles to be achieved by allowing the Mn^{2+} ions to diffuse into the CNT paper uniformly during the rests between the pulses. Fig. 4a and b shows typical time profiles of the applied potential and resulting current density. Fig. 4c–f shows the SEM images of the electrode surface after pulse-deposition by repeatedly applying potential pulses of 2.0 V for 0.5 s at 10 s intervals (15–60 times). Small MnO_2 particles covered the CNT bundles after 15 pulses, and CNT–MnO_2 core–shell wires became thicker after more pulses. SEM images and EDS elemental mapping of the cross-section (Fig. 4g–j and S2c†) show that MnO_2 was uniformly electrodeposited inside the CNT paper. In the case of
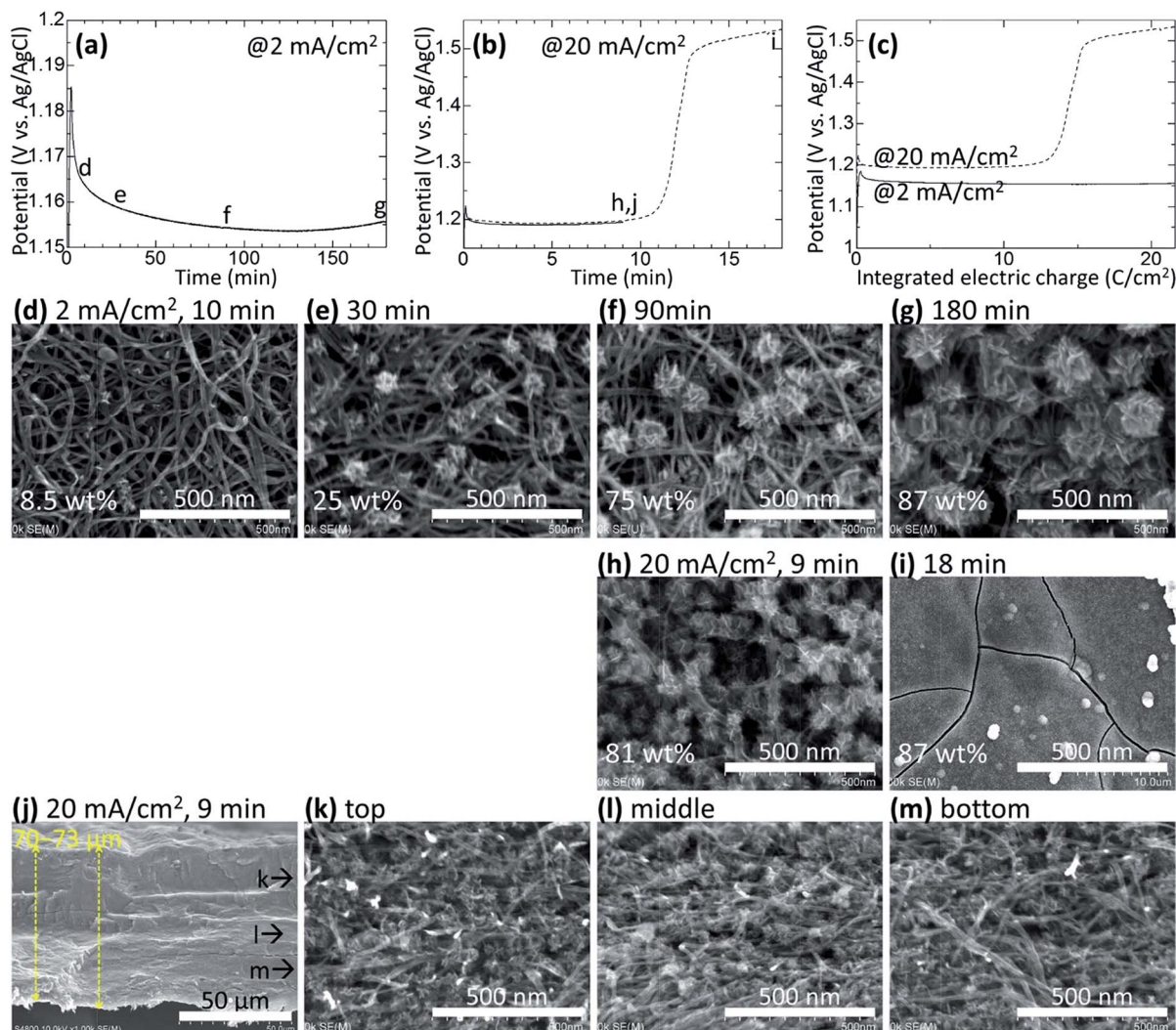
Fig. 3 Electrodeposition of MnO_2 in CNT papers (28–34 μm) by CC of 2 and 20 mA cm^{-2}. The potential change with (a and b) electrodeposition time and (c) integrated electric charge. The potential change is shown for different runs in (b). SEM images of the surfaces of the CNT paper with MnO_2 electrodeposited at (d–g) 2 and (h and i) 20 mA cm^{-2}. A cross-sectional SEM image of (h) is shown in (j–m). SEM-EDS elemental mapping images are shown for the cross-section in Fig. S2b.†

CC, the small current and thus the low potential nucleated MnO_2 particles at a low density resulting in large particles (Fig. 3). Conversely, the high potential pulse-deposition enhanced the nucleation of MnO_2 particles owing to a high overpotential, resulting in small MnO_2 particles at a very high density covering the CNT surfaces.

Fig. S3† shows the XRD spectra of the CNT paper and the composite electrodes after electrodeposition by CP, CC, and Pulse. Peaks corresponding to (100), (101), (102), and (110) of akhtenskite-type MnO_2 are present in all the spectra. The peaks are sharp for MnO_2 electrodeposited by CC, and the full width at half maximum (FWHM) increases in the order of CC, CP, and Pulse, showing that MnO_2 electrodeposited at higher potential results in poorer crystallinity. The peaks of the sample prepared by applying Pulse shifted to lower angles, showing increased lattice spacings and suggesting inferior crystallinity because of the rapid MnO_2 deposition at a high overpotential.

Electrochemical performances of MnO_2–CNT hybrid electrodes

The electrochemical performance of the MnO_2–CNT hybrid electrodes was examined using a three-electrode cell with 1 M Na_2SO_4 aqueous solution at a potential range of 0–0.8 V. Fig. S4† shows typical CV curves of the MnO_2–CNT electrode electrodeposited by CP at 1.20 V for 10 min. The CV curves show rectangular shapes at low scan rates, which are typical of capacitor electrodes and suggest that sufficient electric conduction pathways are provided by the CNT matrix. At higher scan rates $\geq$100 mV s^{-1}, their shapes change to parallelogram, resulting in decreasing capacitances with scan rates.

Fig. 5 shows the rate performances of the MnO_2–CNT hybrid electrodes electrodeposited by CP (Fig. 5a–c), CC (Fig. 5d–f), and Pulse (Fig. 5g–i). The MnO_2-based capacitances (Fig. 5c, f and i) were estimated by subtracting the capacitance of the CNT paper from the total capacitance of the electrodes (Fig. 5b, e and h).
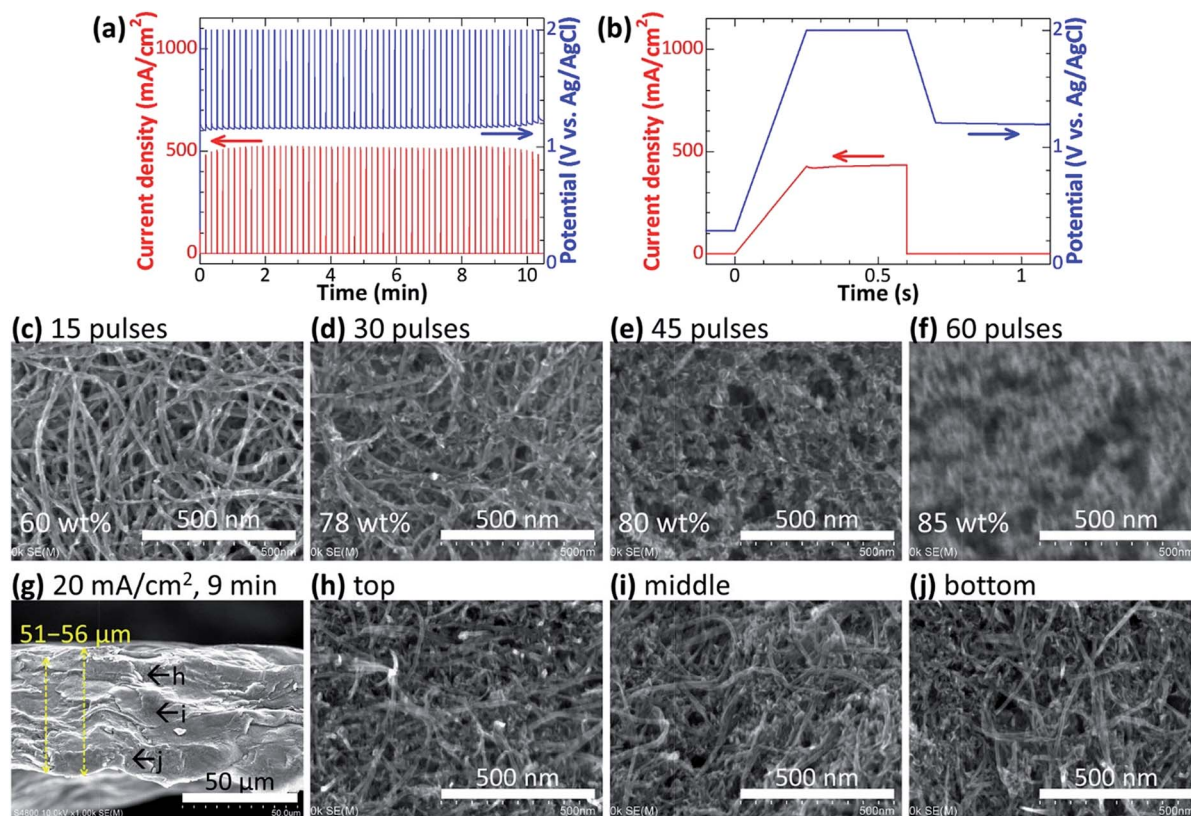
Fig. 4 Electrodeposition of MnO_2 in CNT papers (32–37 μm) by applying potential pulses of 2.0 V. Time profiles of the applied potential and resulting current density for (a) the whole deposition and (b) a single pulse. (c–f) SEM images of the surface of the CNT papers with MnO_2 electrodeposited with 15–60 pulses. (g–j) A cross-sectional SEM image of the MnO_2–CNT hybrid shown in (e). SEM-EDS elemental mapping images for the cross-section are shown in Fig. S2c.†

Because the CNT papers lose their exposed surface as MnO_2 is deposited, the contribution of the CNTs is overestimated and the actual MnO_2-based capacitance should be higher.

The total areal capacitance at 1 mV s^{-1} of the MnO_2–CNT hybrids prepared by CP at 1.20 V increased significantly with deposition time, from 0.02 F cm^{-2} for pristine CNTs to 1.08 F cm^{-2} after 30 min deposition (Fig. 5a). The total gravimetric capacitance at 1 mV s^{-1} increased from 22 F$_{total}$ g$_{electrode}^{-1}$ for pristine CNTs to 124 F$_{total}$ g$_{electrode}^{-1}$ after 10 min deposition, but it changed little at a low scan rate and decreased at a high scan rate after a 30 min deposition (Fig. 5b). The MnO_2-based capacitance was largest after a 2 min deposition (170 and 131 F$_{MnO_2}$ g$_{MnO_2}^{-1}$ at 1 and 200 mV s^{-1}, respectively) and decreased monotonically after deposition for 2 to 30 min (Fig. 5c) owing to the increased particle size of MnO_2 (Fig. 2). Previous reports mainly discuss the gravimetric capacitance of MnO_2, for which the largest value can be obtained for a small MnO_2 load. However, the total capacitance of an electrode is more important for practical applications, and the largest gravimetric and areal capacitances can be obtained for a moderate (10 min) and large (30 min) load of MnO_2, respectively. The MnO_2–CNT hybrid deposited at 1.20 V for 10 min had a large thickness of 62 μm, high areal mass of 6.75 mg cm^{-2} and high mass density of 1.09 g cm^{-3}, yielding a moderate total gravimetric capacitance of 120 and 51 F$_{total}$ g$_{electrode}^{-1}$, high volumetric capacitance of

131 and 56 F$_{total}$ cm^{-3} and high areal capacitance of 0.81 and 0.34 F$_{total}$ cm^{-2} at scan rates of 2 and 200 mV s^{-1}, respectively.

The changes in the capacitance values for the hybrids prepared by CP at 1.30 V were different from those prepared by CP at 1.20 V. The total areal capacitances were largest (0.48 F cm^{-2} at 1 mV s^{-1}) after a 2 min deposition and decreased after further deposition for 10 and 30 min (Fig. 5a). Additional deposition of over 10 min resulted in continuous film formation on the electrode surface (Fig. 2h and i), which inhibited the use of MnO_2 particles inside the CNT papers. A similar change was observed for the total and MnO_2-based gravimetric capacitances (Fig. 5b and c).

For the MnO_2–CNT hybrids prepared by CC at 2 mA cm^{-2}, the total areal capacitance increased with the deposition time (and thus MnO_2 load) (Fig. 5d). The total gravimetric capacitance increased with deposition time, showing a maximum at 90 min and decreasing at 180 min (Fig. 5e). The MnO_2-based gravimetric capacitance decreased monotonically with increasing deposition time owing to the monotonic increase in the particle size of MnO_2 (Fig. 3d–g). The capacitances of the materials obtained by CC at 20 mA cm^{-2} were significantly larger than those obtained by CC at 2 mA cm^{-2} (Fig. 5d–f). The total electric charge for electrodeposition was the same between 2 mA cm^{-2} for 90 min and 20 mA cm^{-2} for 9 min and between 2 mA cm^{-2} for 180 min and 20 mA cm^{-2} for 18 min, yielding
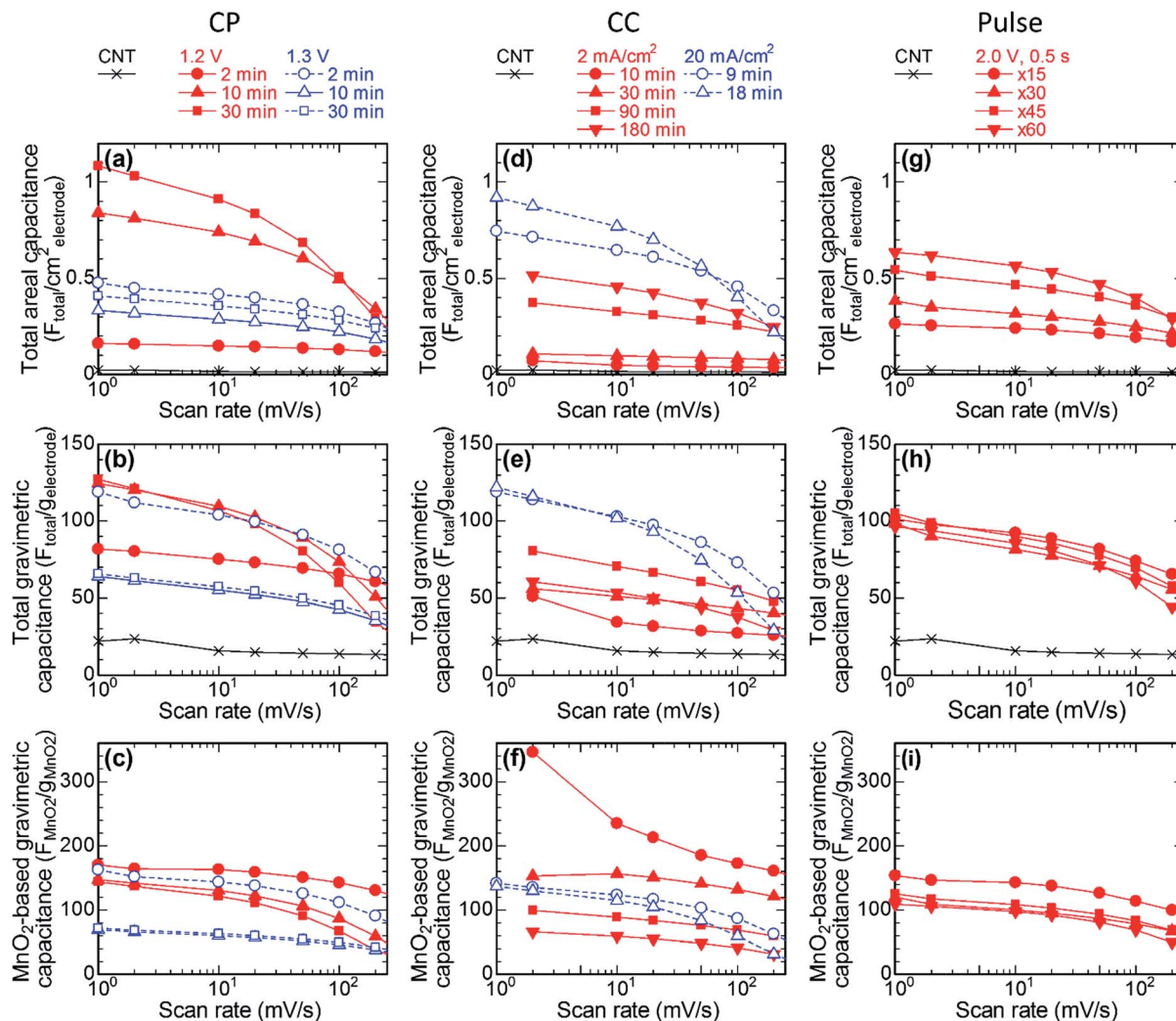
Fig. 5 Rate performances of the hybrids with MnO_2 electrodeposited by CP (a–c), CC (d–f), and Pulse (g–i) on CNT papers of $\sim$30 μm in thickness (0.57–1.28 mg cm^{-2}). (a, d and g) Areal capacitances for the total films (total capacitance divided by electrode area). (b, e and h) Gravimetric capacitances for the total film (total capacitance divided by electrode mass). (c, f and i) Gravimetric capacitances for MnO_2 (the capacitance of pristine CNTs was subtracted from the total capacitance, and then divided by the mass of MnO_2).

similar content of MnO_2 in the hybrid films (75 and 81 wt% for the former and 87 and 87 wt% for the latter). The significantly high capacitance of the hybrids obtained by CC at 20 mA cm^{-2} was attributed to the smaller MnO_2 particles at higher density (Fig. 3h) although a continuous film covers the electrode surface after deposition for 18 min (Fig. 3i). When we carefully compare the two hybrids at 20 mA cm^{-2}, both the total and MnO_2-based capacitances were higher for the hybrid deposited for 9 min than that for 18 min at high scan rates ($\geq$50 mV s^{-1}). The capacitance tends to be limited by the ionic diffusion in electrolyte because more ions need to diffuse through the pores of smaller volume and/or larger tortuosity in the hybrids with higher MnO_2 content. The best conditions change for the targeted capacitances (i.e., areal or gravimetric), and in view of gravimetric capacitance, the best hybrid obtained by CC at 20 mA cm^{-2} for 9 min (Fig. 5e) showed a similar performance with the best hybrid obtained by CP at 1.20 V for 10 min (Fig. 5b). This result is reasonable if we consider the similar

electrodeposition conditions between the former (81 wt% MnO_2 at 20 mA cm^{-2} and $\sim$1.2 V for 9 min, Fig. 3b and h) and the latter (82 wt% MnO_2 at 18–19 mA cm^{-2} and 1.20 V for 10 min, Fig. 2a and e).

For the MnO_2–CNT hybrids prepared by applying Pulse (Fig. 5g), the total areal capacitance also increased with the number of pulses and thus the MnO_2 load, but did not increase as much compared with the hybrids prepared by CP and CC. Their total gravimetric capacitances were fairly high for all of the conditions between 15 and 60 pulses (Fig. 5h); 96–105 and 44–65 F_{total} $g_{electrode}^{-1}$ at 1 and 200 mV s^{-1}, respectively. Their MnO_2-based gravimetric capacitance showed some decrease with increasing number of pulses; from 154 to 109 and from 100 to 49 F_{MnO_2} $g_{MnO_2}^{-1}$ at scan rates of 1 and 200 mV s^{-1} for 15 and 60 pulses, respectively. Because of the smaller MnO_2 particles electrodeposited by Pulse, the MnO_2-based gravimetric capacitance did not change much (Fig. 5i), resulting in almost constant total gravimetric capacitances (Fig. 5h) and increasing

total areal capacitances (Fig. 5g) with increasing number of pulses and thus MnO_2 load. But the inferior crystallinity of the MnO_2 particles prepared by Pulse compared with those prepared by CP and CC (Fig. S3†) may have cancelled the advantage of small particle size, resulting in moderate MnO_2-based gravimetric capacitance values. Further enhancement of the capacitances could be expected by improving the crystallinity of MnO_2 by adjusting the potential more carefully.

Fig. 6 summarizes the capacitance of our MnO_2–CNT hybrid electrodes electrodeposited under various conditions. Fig. 6a clearly shows that the total areal capacitance increased with MnO_2 load under most conditions, and largest values were achieved for the films by CP at 1.20 V and CC at 20 mA cm^{-2}. Fig. 6b shows that the total gravimetric capacitance increased with MnO_2 load of ≤3 mg cm^{-2} but became saturated or even decreased for higher MnO_2 load. The capacitance enhancement is more significant than the mass increase for small MnO_2 load but the mass increase becomes more significant than capacitance enhancement for large MnO_2 load. Fig. 6c shows that the MnO_2-based gravimetric capacitance was very high for very small MnO_2 load (346 F$_{MnO_2}$ g$_{MnO_2}^{-1}$ at 2 mV s^{-1} for a hybrid with MnO_2 load of 0.12 mg cm^{-2} and 8.5 wt%), which decreased monotonically to 30–150 F$_{MnO_2}$ g$_{MnO_2}^{-1}$ with increasing MnO_2 load. The utility ratio of MnO_2 decreased with increasing MnO_2 load owing to the increasing particle size, increasing tortuosity, decreasing porosity, and/or continuous film formation (Fig. 2–4). Fig. 6d shows the film performance plotted

against the capacitance values that are important for practical application; total areal capacitance *vs.* total gravimetric capacitance. The hybrids deposited by CP at 1.20 V for 10 and 30 min and those deposited by CC at 20 mA cm^{-2} for 9 and 18 min showed high gravimetric and areal capacitances at low scan rates of 2–20 mV s^{-1} owing to the high load. In contrast, they showed a decreased capacitance at a high scan rate of 200 mV s^{-1} owing to the large particle size and/or continuous surface layer of MnO_2 (Fig. 3 and 4). The hybrids deposited by applying Pulse with 45 and 60 pulses showed moderately high gravimetric and areal capacitances. Fig. 6e shows the film performance plotted against the total areal capacitance and MnO_2-based gravimetric capacitance. It is clear that the MnO_2-based gravimetric capacitance, which is often called "specific capacitance" and reported as a primary property, is in a tradeoff relationship with the areal capacitance that is important for practical applications. Fig. 1e shows a similar plot comparing the present work with previous reports in a logarithmic scale with a different definition of the gravimetric capacitance (*i.e.*, MnO_2-based capacitance divided by MnO_2 mass for Fig. 6e and total capacitance divided by MnO_2 mass for Fig. 1e). Encouraging values that were reported for MnO_2-based gravimetric capacitance were realized by very small MnO_2 loads, resulting in very small total areal capacitance values. Our electrodes with fine MnO_2 particles uniformly electrodeposited in 18–37 μm thick CNT paper realized areal capacitance of ∼1 F cm^{-2}, which is much higher than most of previously reported values.
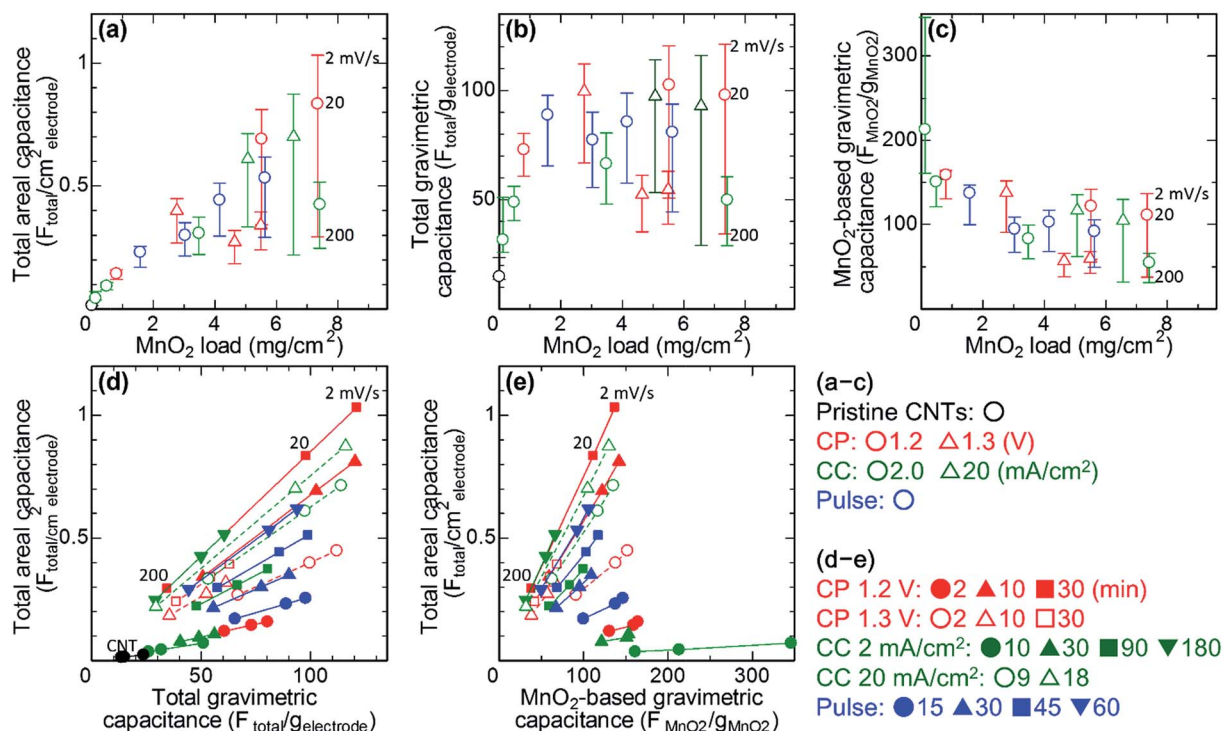

Fig. 6 Summary of the capacitance of MnO_2–CNT hybrid electrodes deposited under various conditions. (a) Total areal capacitance, (b) total gravimetric capacitance, and (c) MnO_2-based gravimetric capacitance were plotted against MnO_2 load. Plots show the capacitance values at a scan rate of 20 mV s^{-1}, and error bars show the values at scan rates of 2 and 200 mV s^{-1}. Total areal capacitance was plotted against (d) total gravimetric capacitance and (e) MnO_2-based gravimetric capacitance. Capacitances at scan rates of 2, 20, 200 mV s^{-1} of the same film were plotted with the same symbol and connected with a line.

Stability and performance changes of the MnO_2–CNT hybrid electrodeposited by CP at 1.20 V for 10 min were tested by galvanostatic charge–discharge cycling between 0.0 and 0.8 V. The symmetric shape of the charge–discharge profiles is very close to that expected for an ideal capacitor, with small *IR* (current–resistance) drops (Fig. S5a†). As for the cycle stability, the electrode showed some decay in capacitance to ~90% after 5000 cycles (Fig. S5b†).

Conclusions

MnO_2–CNT hybrid electrodes were fabricated by electrodepositing MnO_2 on self-supporting CNT paper as a three dimensional current collector. For uniform electrodeposition of MnO_2 particles inside the 18–37 μm-thick CNT papers, we considered diffusion and reaction processes of Mn^{2+} ions. A high potential enhanced the reaction, especially nucleation of MnO_2 particles, yielding small particles at high density. But the process was diffusion-controlled, yielding a dense MnO_2 layer on the exterior surface of the electrodes. Such electrodes were not suitable for capacitor electrodes because of the inhibited ionic diffusion by the dense layer during capacitor operation. In contrast, a low potential made the reaction slow, making the process reaction controlled and realizing uniform MnO_2 deposition within the CNT matrix owing to the sufficient Mn^{2+} diffusion. But the low potential made the nucleation of MnO_2 particles slow, yielding large particles at a low density. Such electrodes did not show high capacitance owing to the low electric conductivity of MnO_2 and slow ionic diffusion in MnO_2. To overcome the tradeoff between the uniformity and particle size/density, we examined pulse electrodeposition, in which high potential pulses were intermittently applied to deposit fine MnO_2 particles at high density and allow the Mn^{2+} ions to diffuse during the intervals. MnO_2 was deposited uniformly with amounts increasing roughly proportional to the charge, and we obtained electrodes with MnO_2 content of ≥80 wt% (and thus CNT ≤ 20 wt%) without the formation of a dense MnO_2 layer on the electrode surface.

For the electrodes using 18–37 μm-thick CNT paper, the best performance was achieved when MnO_2 was deposited by CP of 1.20 V for 10 min. The resulting MnO_2–CNT hybrid had a large thickness of 62 μm, high areal mass of 6.75 mg cm^{-2} and high mass density of 1.09 g cm^{-3}, yielding a moderate total gravimetric capacitance of 120 and 51 F_{total} g$_{electrode}$$^{-1}$, high volumetric capacitance of 131 and 56 F_{total} cm^{-3} and high areal capacitance of 0.81 and 0.34 F_{total} cm^{-2} at scan rates of 2 and 200 mV s^{-1}, respectively. The MnO_2–CNT hybrid prepared by Pulse had small particles at high density uniformly dispersed within the CNT matrix, but showed moderate capacitance possibly owing to the inferior crystallinity resulting at the high applied potential of 2.0 V. We are trying to improve the crystallinity of the small MnO_2 particles deposited uniformly at high density by adjusting the potential used for the pulse deposition.

Acknowledgements

Notes and references

1 J. P. Zheng, P. J. Cygan and T. R. Jow, *J. Electrochem. Soc.*, 1995, **142**, 2699.

2 D. B. Rogers, R. D. Shannon, A. W. Sleight and J. L. Gillson, *Inorg. Chem.*, 1969, **8**, 841.

3 S. Hadi-Jordanov, H. Angerstein-Kozlowska, M. Vuković and B. E. Conway, *J. Electrochem. Soc.*, 1978, **125**, 1471.

4 N.-L. Wu, S.-L. Kuo and M.-H. Lee, *J. Power Sources*, 2002, **104**, 62.

5 G. Wang, L. Zhang and J. Zhang, *Chem. Soc. Rev.*, 2012, **41**, 797.

6 G. Yu, L. Hu, N. Liu, H. Wang, M. Vosgueritchian, Y. Yang, Y. Cui and Z. Bao, *Nano Lett.*, 2011, **11**, 4438.

7 M. Toupin, T. Brousse and D. Belanger, *Chem. Mater.*, 2004, **16**, 3184.

8 M. Yano, S. Suzuki, M. Miyayama and M. Ohgaki, *Solid State Ionics*, 2013, **233**, 32.

9 G. Wang, L. Zhang and J. Zhang, *Chem. Soc. Rev.*, 2012, **41**, 797.

10 S. R. Sivakkumar, J. M. Ko, D. Y. Kim and G. C. Wallace, *Electrochim. Acta*, 2007, **52**, 7377.

11 K.-W. Nam, C. Lee, X. Yang, B. W. Cho, W. Yoon and K. Kim, *J. Power Sources*, 2009, **188**, 323.

12 Y. Hou, T. Cheng, T. Hobson and J. Liu, *Nano Lett.*, 2010, **10**, 2727.

13 J.-H. Kim, K. H. Lee, L. J Overzet and G. S. Lee, *Nano Lett.*, 2011, **11**, 2611.

14 L. Hu, W. Chen, X. Xie, N. Liu, Y. Yang, H. Wu, Y. Yao, M. Pasta, H. N. Alshareef and Y. Cui, *ACS Nano*, 2011, **5**, 8904.

15 D. Y. Kim, H. Sugime, K. Hasegawa, T. Osawa and S. Noda, *Carbon*, 2011, **49**, 1972.

16 Z. Chen, D. Y. Kim, K. Hasegawa, T. Osawa and S. Noda, *Carbon*, 2014, **80**, 339.

17 S. W. Lee, B. M. Gallant, Y. Lee, N. Yoshida, D. Y. Kim, Y. Yamada, S. Noda, A. Yamada and Y. Shao-Horn, *Energy Environ. Sci.*, 2012, **5**, 5437.

18 J. C. Bachman, R. Kavian, D. J. Graham, D. Y. Kim, S. Noda, D. G. Nocera, Y. Shao-Horn and S. W. Lee, *Nat. Commun.*, 2015, **6**, 7040.

19 T. Liu, R. Kavian, Z. Chen, S. S. Cruz, S. Noda and S. W. Lee, *Nanoscale*, 2016, **8**, 3671.

20 R. Quintero, D. Y. Kim, K. Hasegawa, Y. Yamada, A. Yamada and S. Noda, *RSC Adv.*, 2015, **5**, 16101.

21 R. Quintero, D. Y. Kim, K. Hasegawa, Y. Yamada, A. Yamada and S. Noda, *RSC Adv.*, 2014, **4**, 8230.

22 W. Xiao, H. Xia, J. Y. H. Fuh and L. Lu, *J. Power Sources*, 2009, **193**, 935.

23 A. Burke, *J. Power Sources*, 2000, **91**, 37.

24 M. Min, K. Machida, J. H. Jang and K. Naoi, *J. Electrochem. Soc.*, 2006, **153**, A334.

25 I. Zhitomirsky, M. Cheong and J. Wei, *JOM*, 2007, **59**, 66.

26 S.-L. Kuo and N.-L. Wu, *J. Electrochem. Soc.*, 2006, **153**, A1317.

27 N. Nagarajan, H. Humadi and I. Zhitomirsky, *Electrochim. Acta*, 2006, **51**, 3039.

28 Y. Jiang, P. Wang, X. Zang, Y. Yang, A. Kozinda and L. Lin, *Nano Lett.*, 2013, **13**, 3524.

29 Y. Jin, H. Chen, M. Chen, N. Liu and Q. Li, *ACS Appl. Mater. Interfaces*, 2013, **5**, 3408.